IAEA
International Atomic Energy Agency

The IAEA ultra-high vacuum chamber at Elettra

Alessandro Migliori

Nuclear Science and Instrumentation Laboratory

International Atomic Energy Agency

IAEA
International Atomic Energy Agency

The joint IAEA-Elettra XRF beamline at Elettra Sincrotrone Trieste

❑ Optical layout

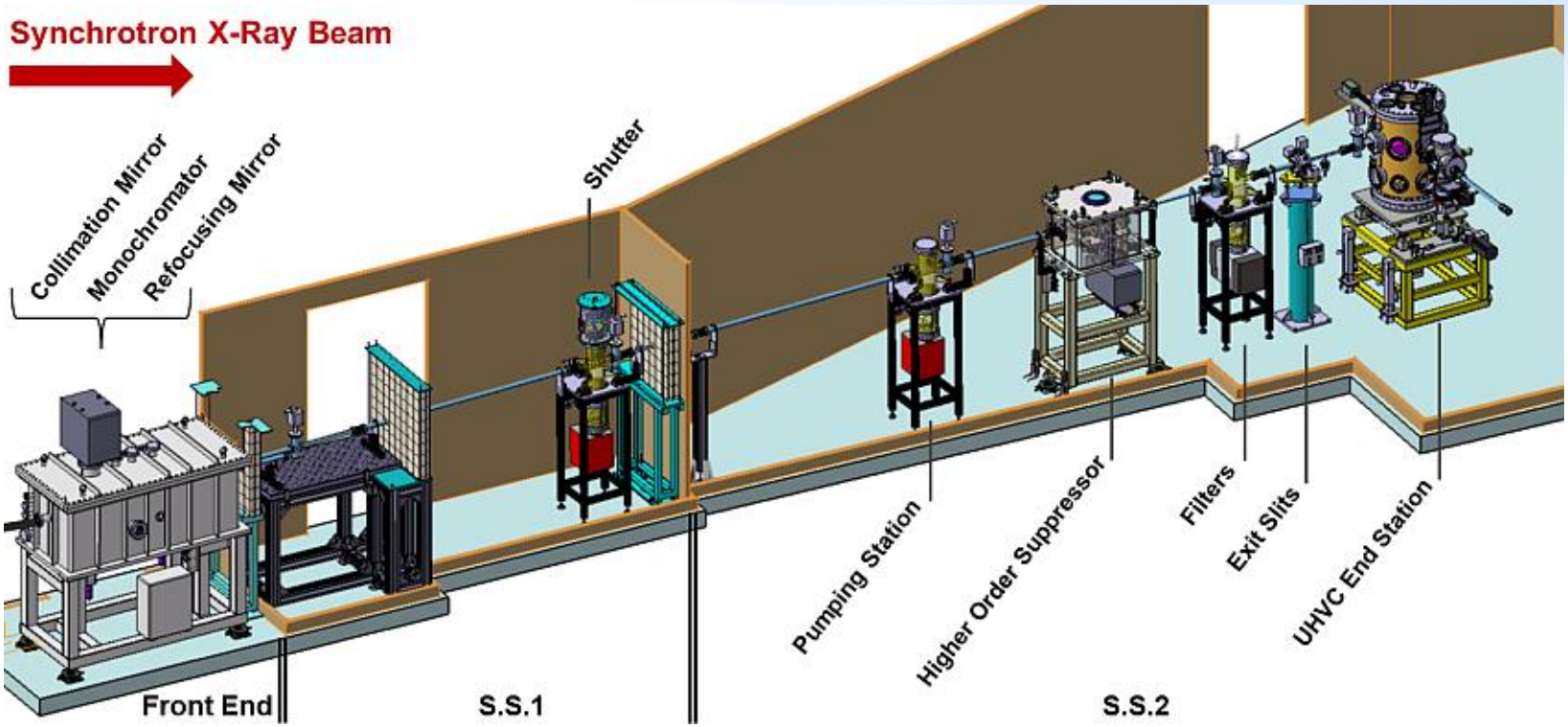

Source	**Bending magnet**
Flux	10^{10}ph/s(at 5 keV for 2.0 GeV, at 10 kev for 2.4 GeV) (Si 111)
Spot size	min **250 x 100 (H x V) µm²**
Beam divergence	< 0.15 mrad (at exit slits)

Werner Jark, Diane Eichert, Lars Luehl, Alessandro Gambitta, *Optimisation of a compact optical system for the beam transport at the x-ray fluorescence beamline at Elettra for experiments with small spots*, Proc. SPIE 9207, Advances in X-Ray/EUV Optics and Components IX, 92070G, 2014; doi: 10.1117/12.2063009

The monochromator at XRF

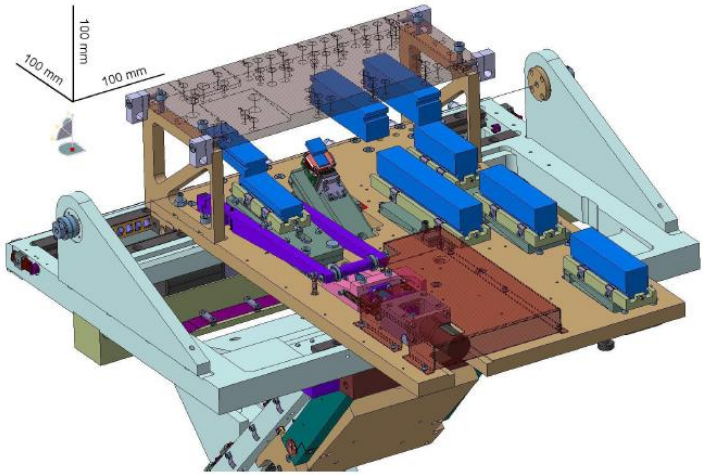

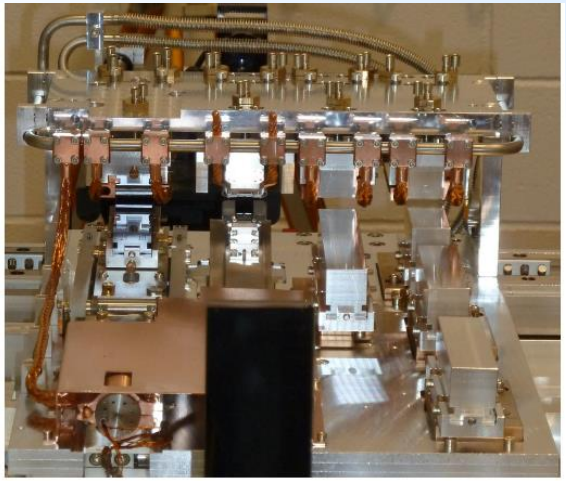

Optics type	E range (keV)	E resolution (ΔE)
Si(111)	3.6 - 14	~ 1 eV at 7 keV
InSb(111)	2.0 – 3.8	~ 1eV at 2.2 keV
ML: High E (RuB_4C)	4.0 – 14.0	~ 55 eV at 1 keV ~ 180 eV at 14 keV
ML: Medium E (NiC)	1.5 – 8.0	
ML: Low E (RuB_4C)	0.7 – 1.8	

Werner Jark *et al.*, Proc. SPIE 9207, Advances in X-Ray/EUV Optics and Components IX, 92070G, 2014; doi: 10.1117/12.2063009

IAEAXspe endstation

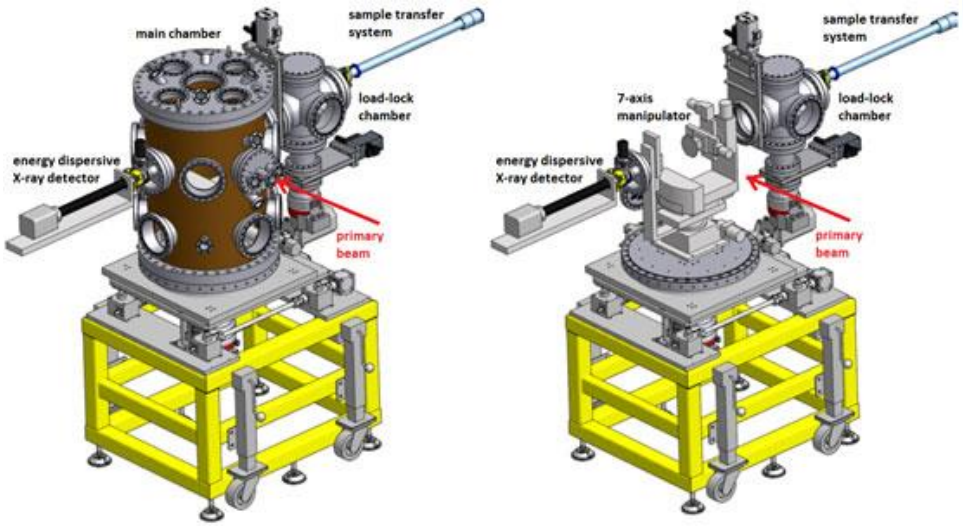

The IAEA end-station is based on a prototype design by Physikalisch - Technische Bundesanstalt (PTB, Berlin) and Technical University of Berlin (TUB)

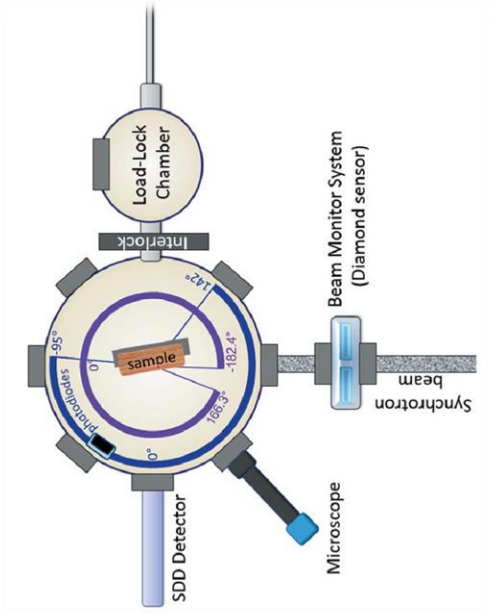

Available detectors:

- Diamond detector for I_0
- SDD detector for **XRF** (different variants) and **XAS** (in fluorescence geometry)
- Photodiodes for **XAS** in transmission geometry
- Photodiodes with 100 and 200µm slits and SDD for **XRR**

Andreas G. Karydas et al., J. Synchrotron Rad. (2018). **25**, 189–203

❑ 7-Axis Manipulator

Sample arm
- 3 linear stages (X, Y, Z)
- 2 goniometers (Theta, Phi)

Photodiodes arm:
- 1 linear stages (diode)
- 1 goniometer (2Theta)

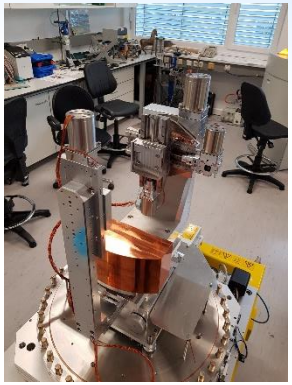

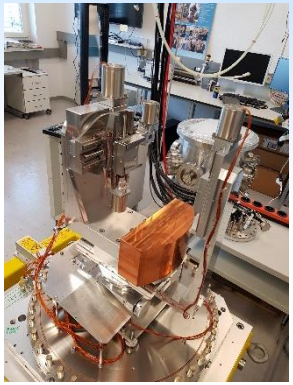

- Sample can be moved in various directions/ orientations with respect to the exciting X-ray beam or with respect to the detectors.

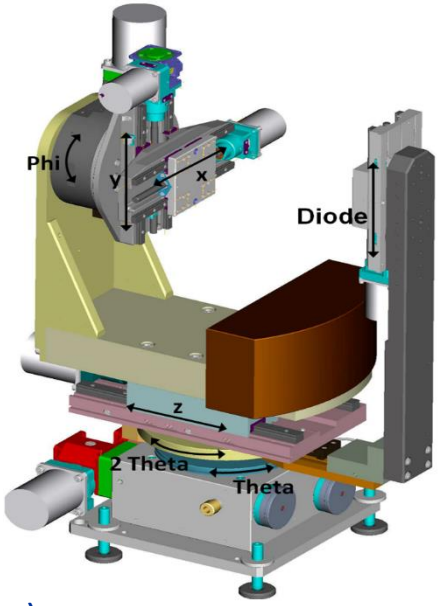

- Ultra Thin Window (UTW) Bruker Silicon Drift detector (30 mm^2, FWHM 131 eV @ Mn-Ka), Si photodiodes

Full step resolution
Linear axes: Diode, X, Y, Z (0.005mm, 0.005mm, 0.0005mm, 0.01mm)
Goniometers: Theta, 2theta, phi (0.001°, 0.001°, 0.005°)

❑ IAEA Coordinated Research Project

- **Materials Science**: Structured materials for energy storage and conversion technologies
- **Nanomedicine - Biosensing technologies**
- **Environmental monitoring** (air particulate matter, water)
- **Biological:** Elemental distribution/ speciation on plant organ (leaves, roots, shoots, seeds, etc.)
- **Cultural Heritage –preventive conservation**
- **Food products security – Authenticity**
- **Determination of X-Ray Fundamental Parameters**

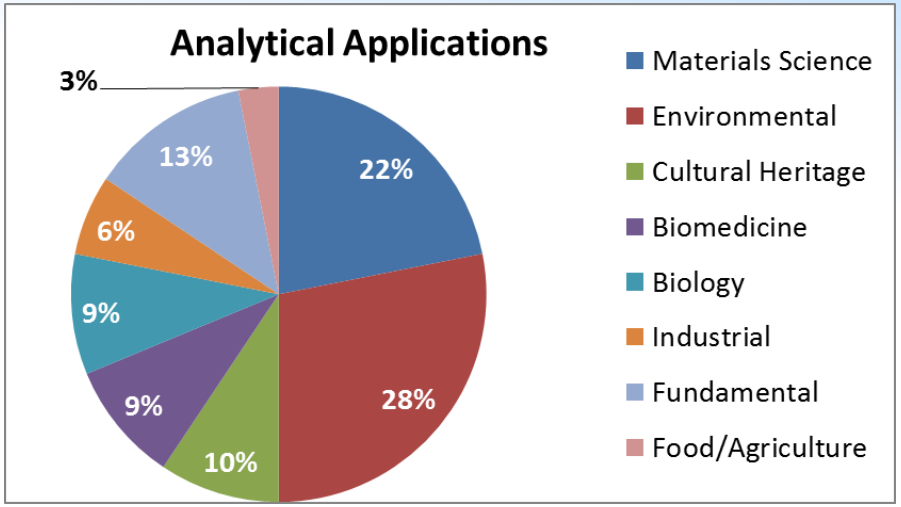

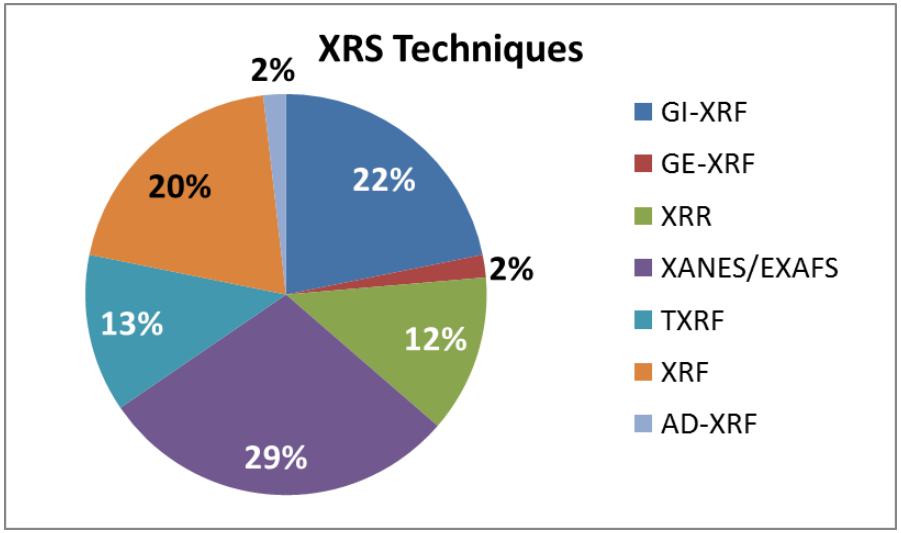

non-UHV compatible samples

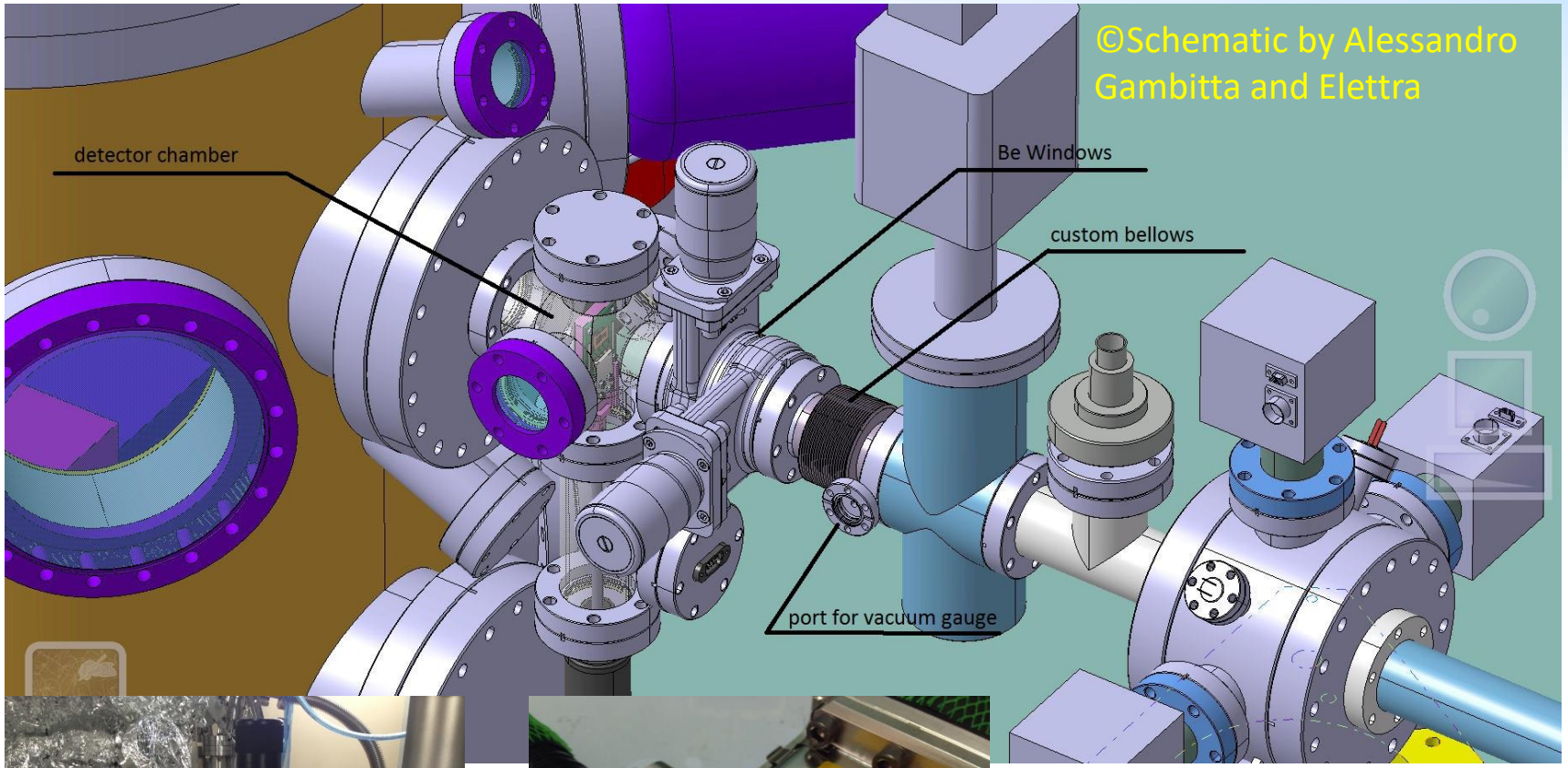

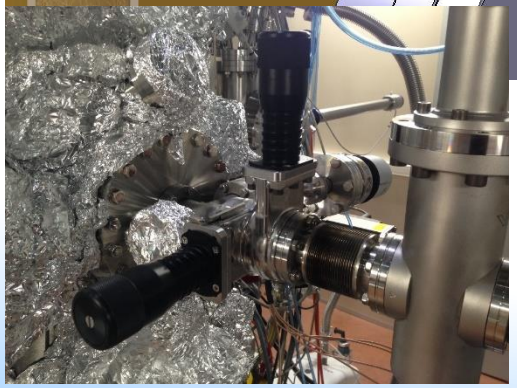

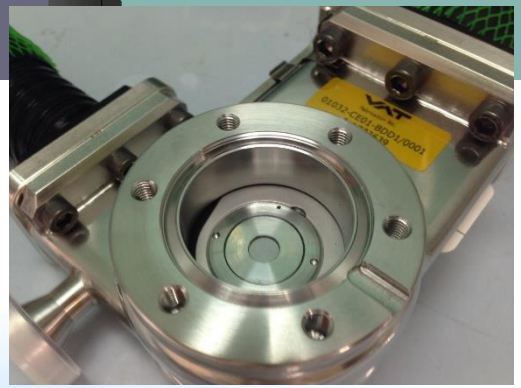

20µm IF-1 Beryllium
Luxel Corporation

Conventional XRF

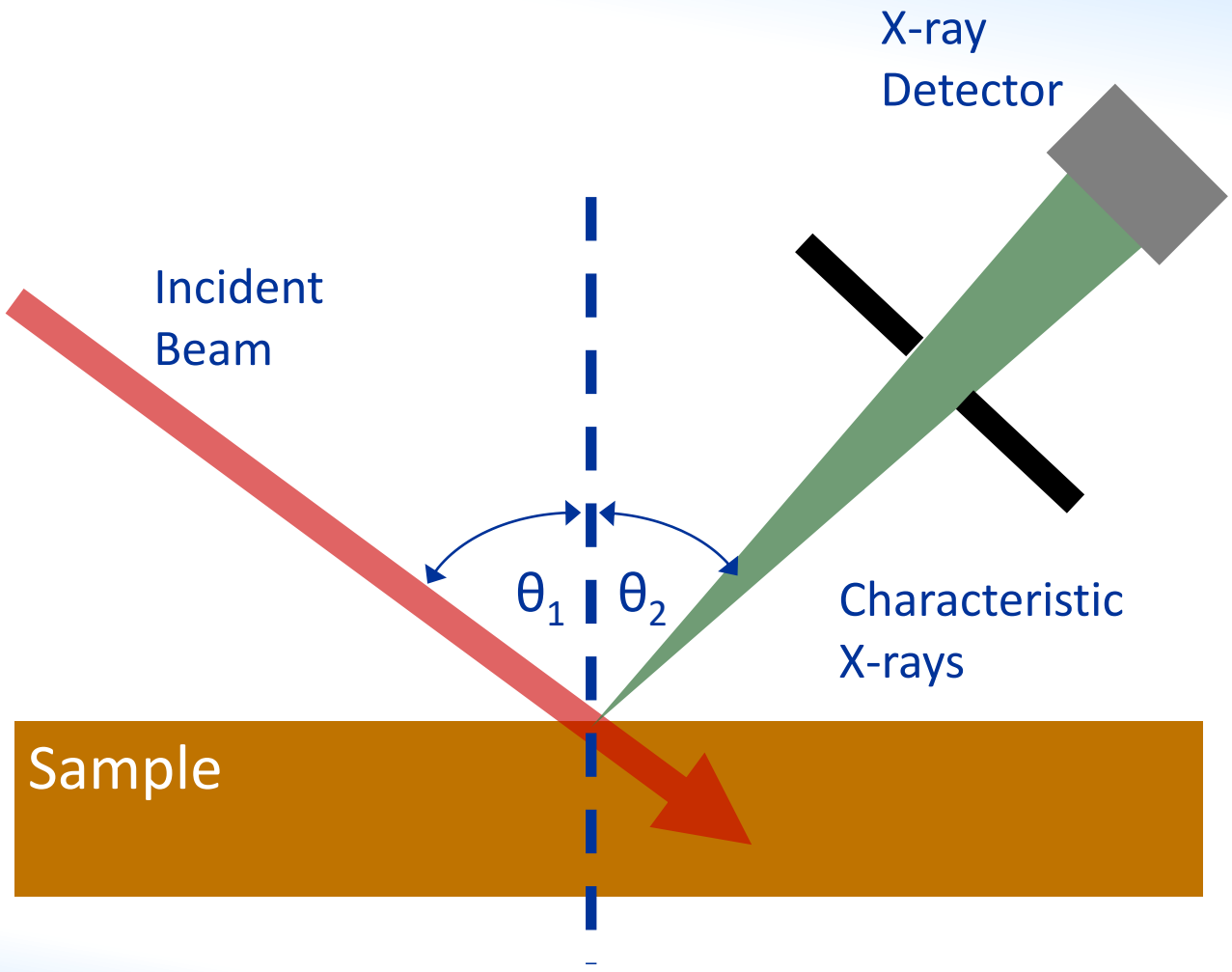

Geometries and techniques

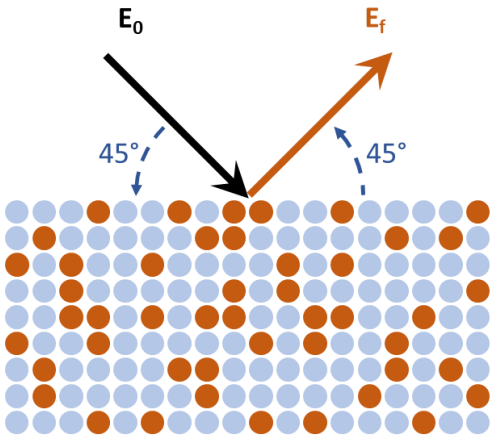

Standard 45°/45° - XRF

Elemental characterization

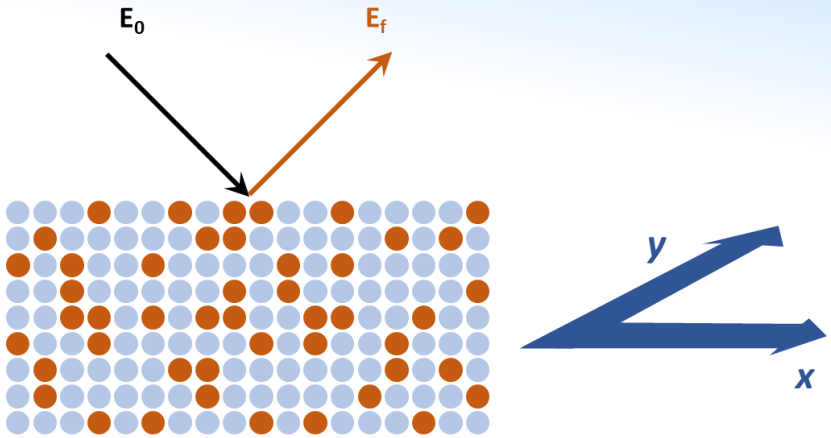

micro - XRF

Mapping

X-ray Absorption Spectroscopy
(on hot spots)

X-ray total reflection

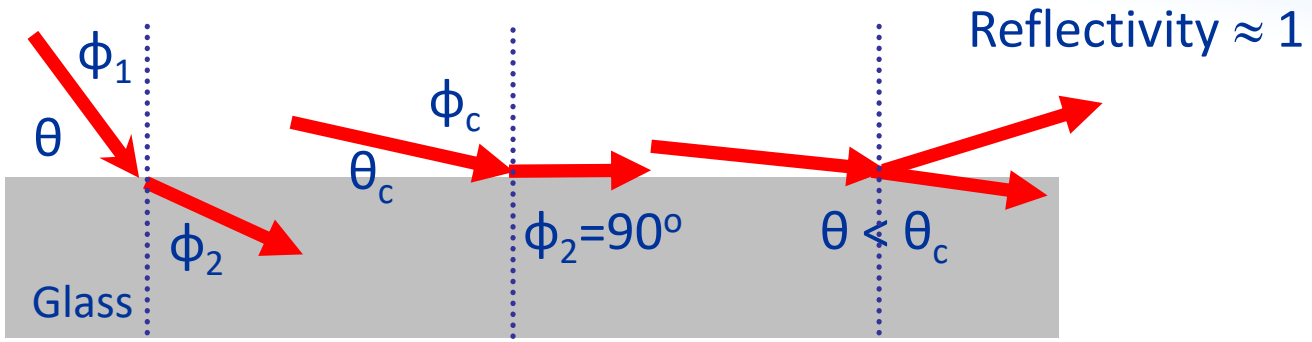

Snell Law $\frac{\sin\phi_2}{\sin\phi_1} = \frac{1}{n} \Rightarrow \sin\phi_2 = \frac{\sin\phi_1}{n} \Rightarrow \phi_2 > \phi_1 \qquad n \approx 1 - \delta$

$\vartheta_{crit} = \sqrt{2\delta}$ $\qquad \vartheta_{crit}(deg) \approx \frac{1.651}{E(keV)}\sqrt{\frac{Z}{A}\rho(\frac{g}{cm^3})}$

Z: Atomic number
A: Atomic mass
ρ: Density

X-ray Standing Wave

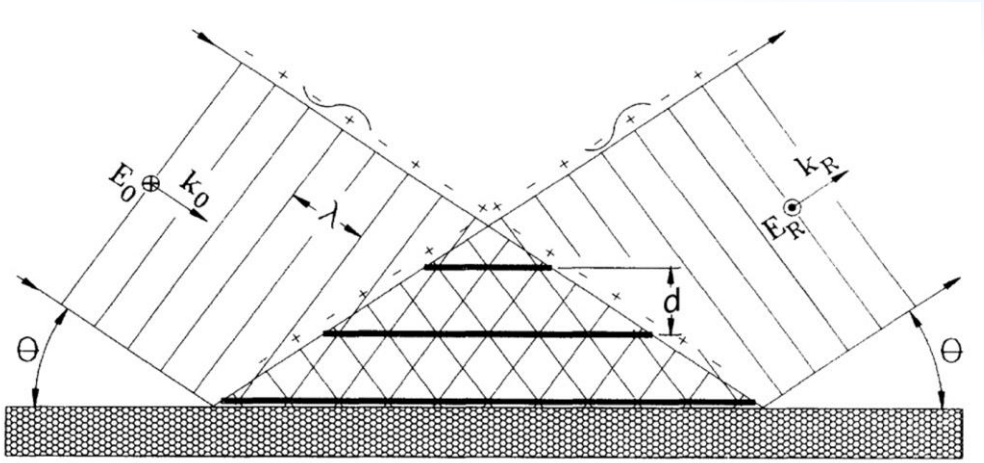

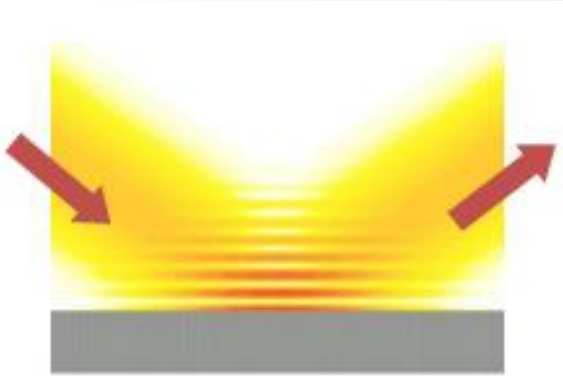

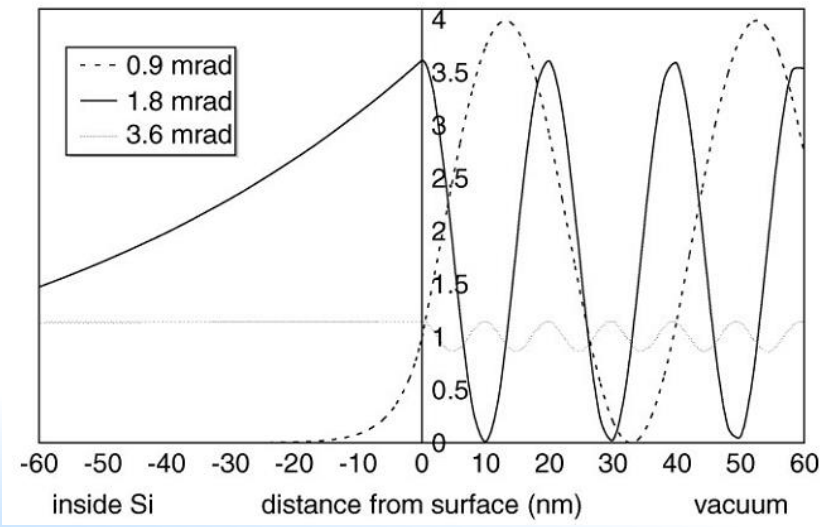

Formation of X-ray Standing Wave (XSW) at grazing incident/exit angle

Electric Field Modulations above the surface

The X-ray fluorescence intensity from the sample depends on the varying field intensity of the XSW field within the sample

GIXRF and XRR

By varying continuously the grazing incident angle through and few times above the critical angle for TR, the recorded XRF intensity profiles (Grazing Incidence-XRF analysis) have the potential to provide information on structural and compositional properties of thin films, such as the layer composition, sequence, thicknesses and densities, interface roughness, in depth elemental gradients of matrix elements or dopants in semiconductors, characterization of nano-particles deposited on flat surfaces, etc

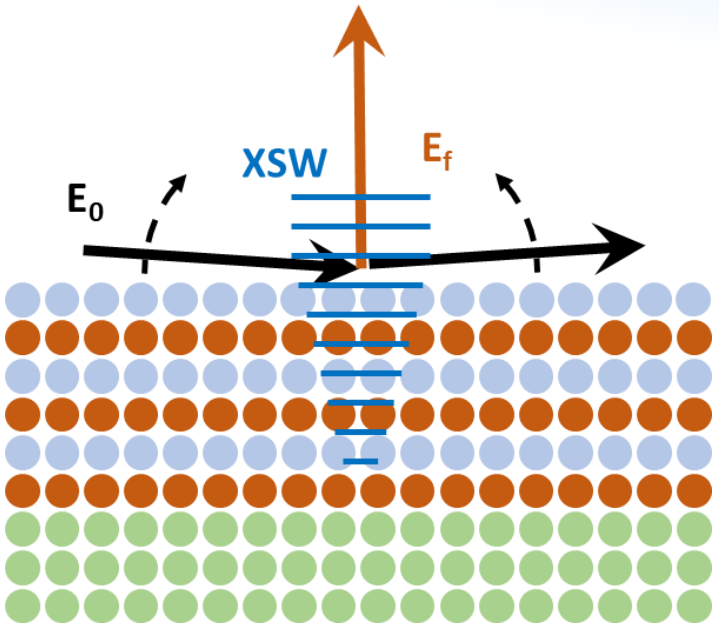

A more accurate and robust reconstruction of these thin film properties requires the synergy or even the simultaneous fitting of GI-XRF with X-ray reflectometry (XRR) data

Total reflection X-ray Fluorescence

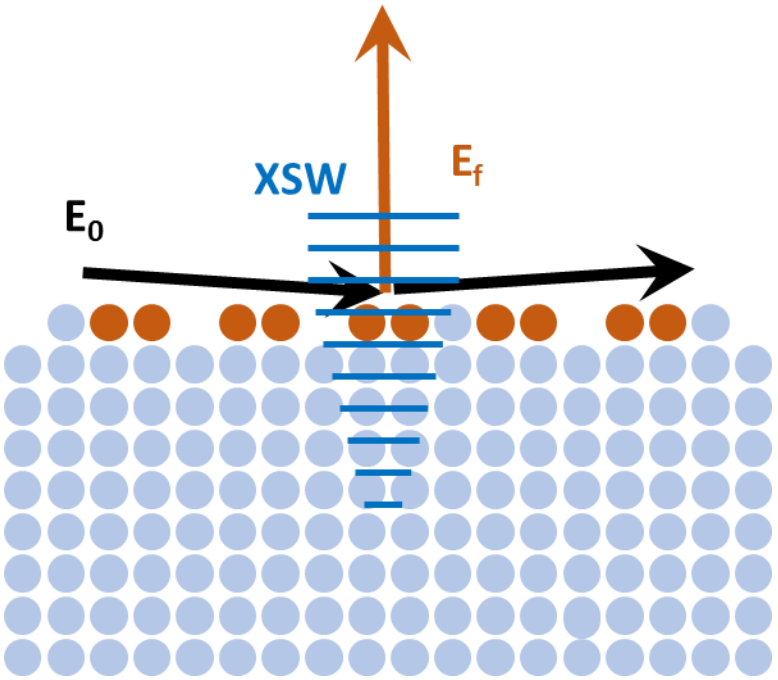

TXRF is essentially an energy dispersive XRF technique arranged in a special geometry.

Due to this configuration, the measured spectral background in TXRF is less than in conventional XRF. This reduction results in increased signal to noise ratio.

TXRF is a surface elemental analysis technique often used for the ultra-trace analysis of particles, residues, and impurities on smooth surfaces.

Fluorescence signal

Signal from particles and thin layers

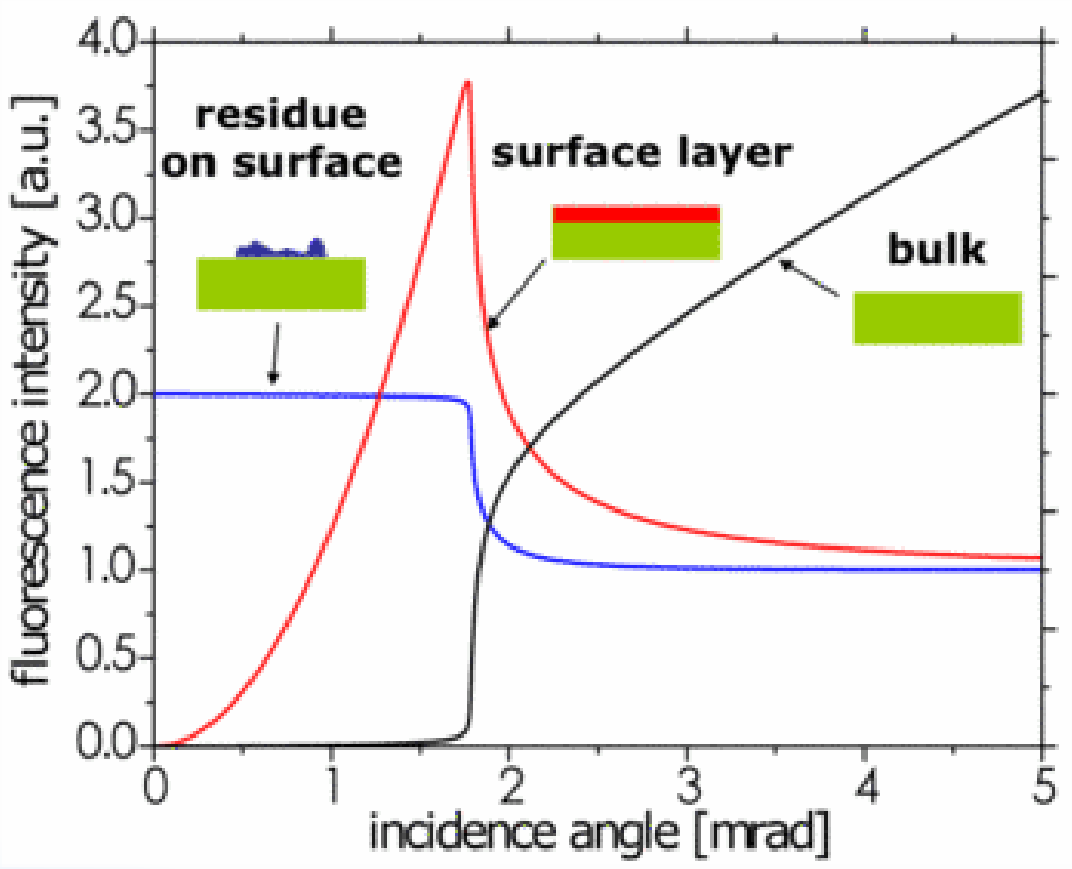

Grazing angle geometries

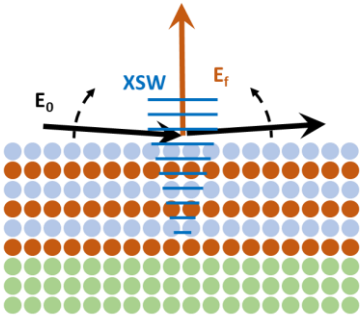

Grazing Incident - XRF

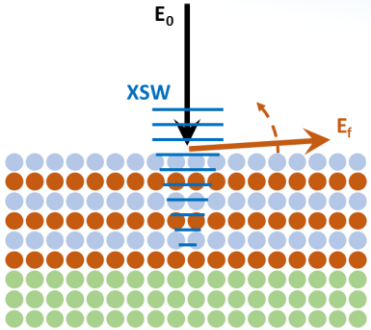

Grazing Emission - XRF

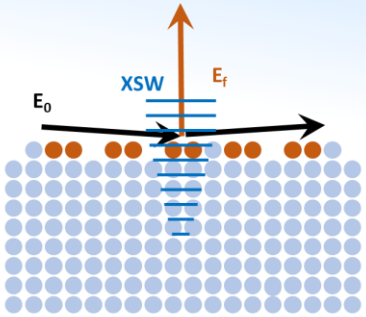

Total reflection - XRF

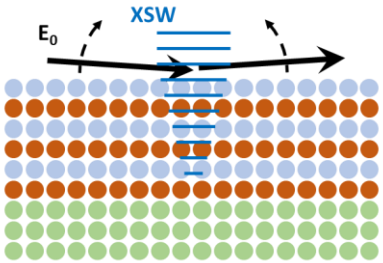

X-Ray Reflectometry

Depth profiling measurements

Trace element analysis
Surface contamination

X-ray Absorption Spectroscopy (in TXRF geometry)

GIXRF Geometry aspects

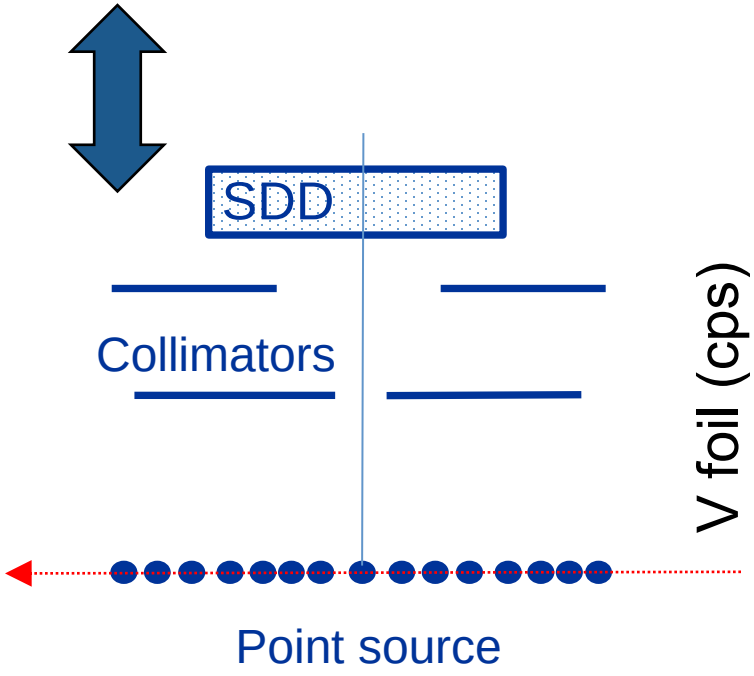

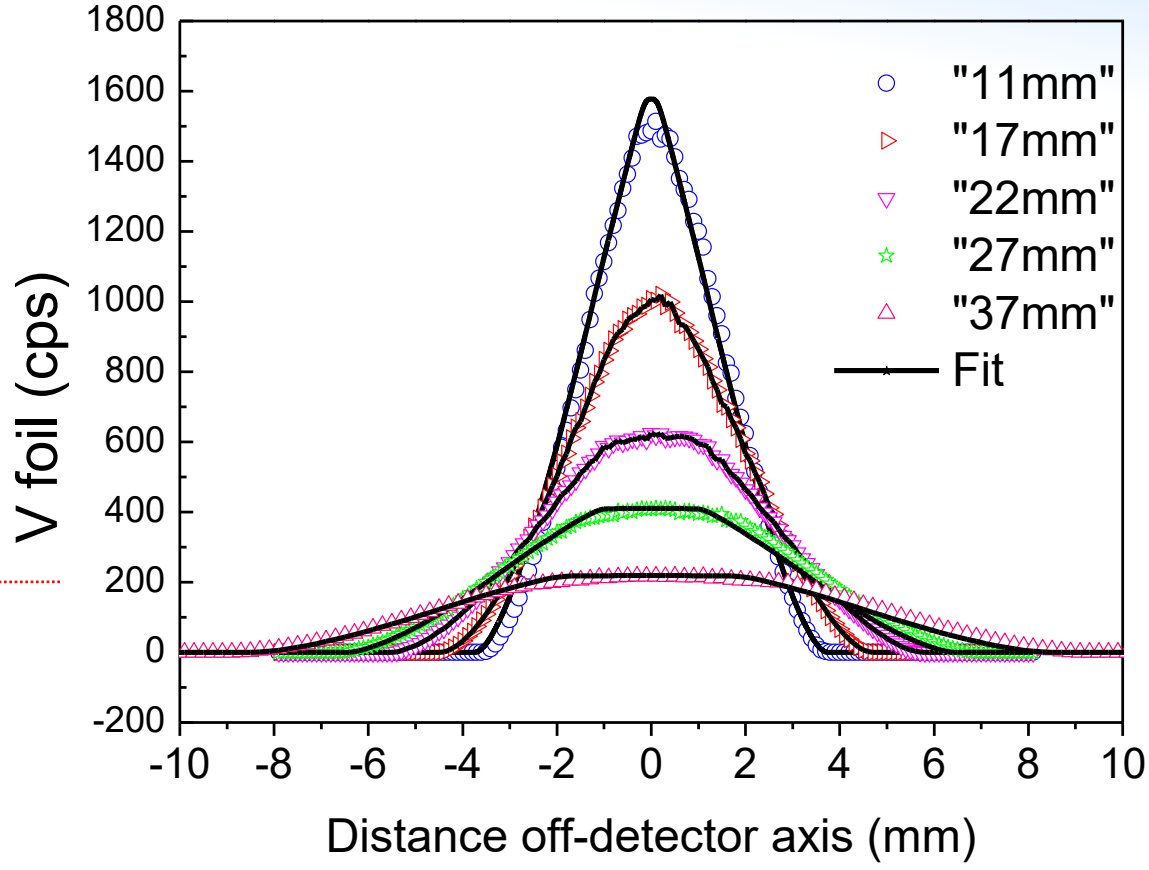

2.25 mm and 4.7 mm collimators

SDD analysis modes (UTW/Be+UTW)

X-ray detector efficiency

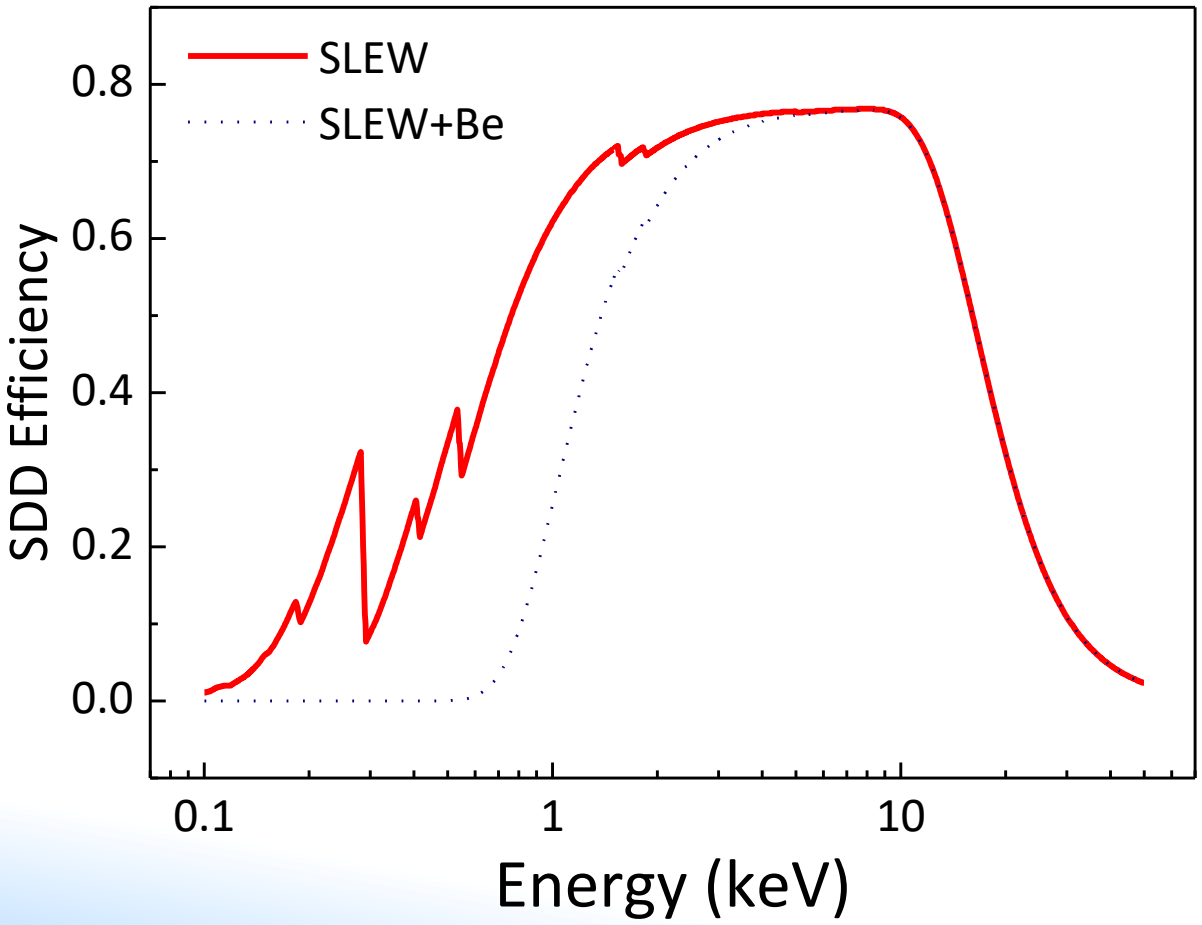

Elemental XRF sensitivities

10 mins measurement, 2.4 GeV mode

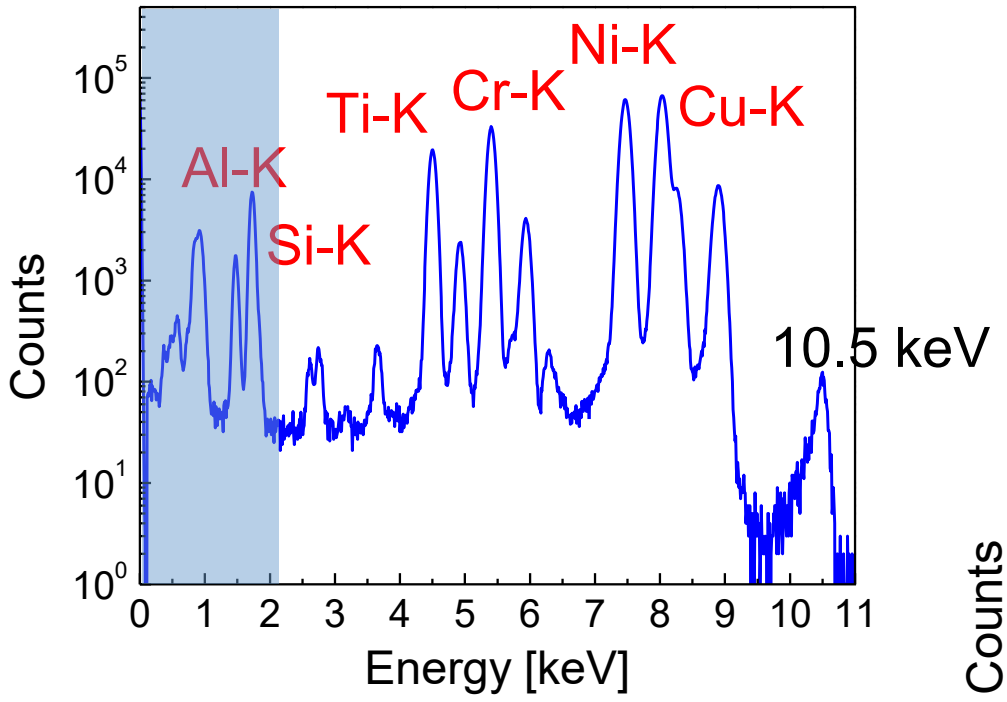

Beam dimensions @ 10.5 keV
260 um (H) 110 um(V)

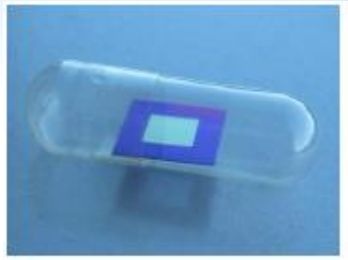

AXO Dresden

Cr/Al/Ni/Cu/Ti/ Si_3N_4 200 nm, each layer about 10 ug/cm²

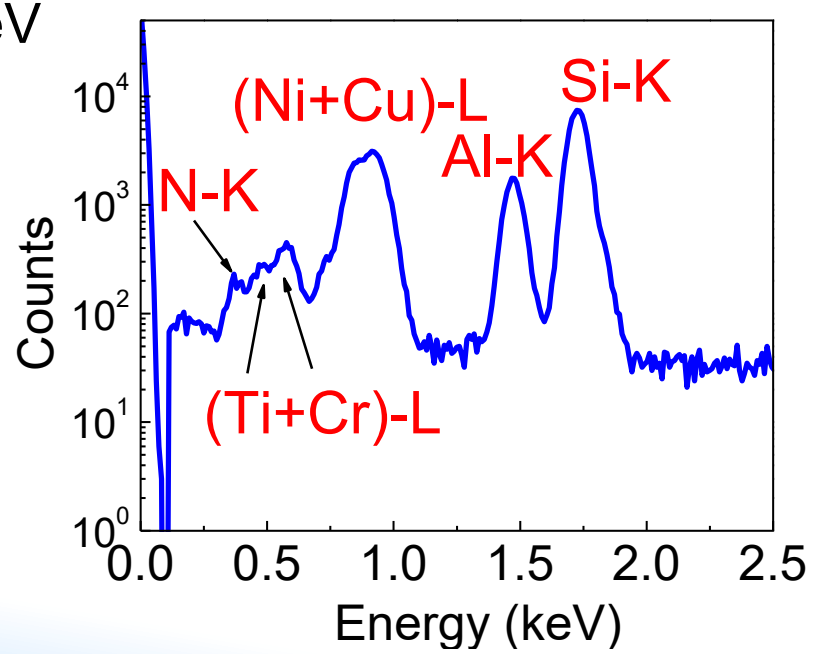

Detection limits from thin sample

Si_3N_4 200 nm membrane, with 10ug/cm² of Cr/Al/Ni/Cu/Ti

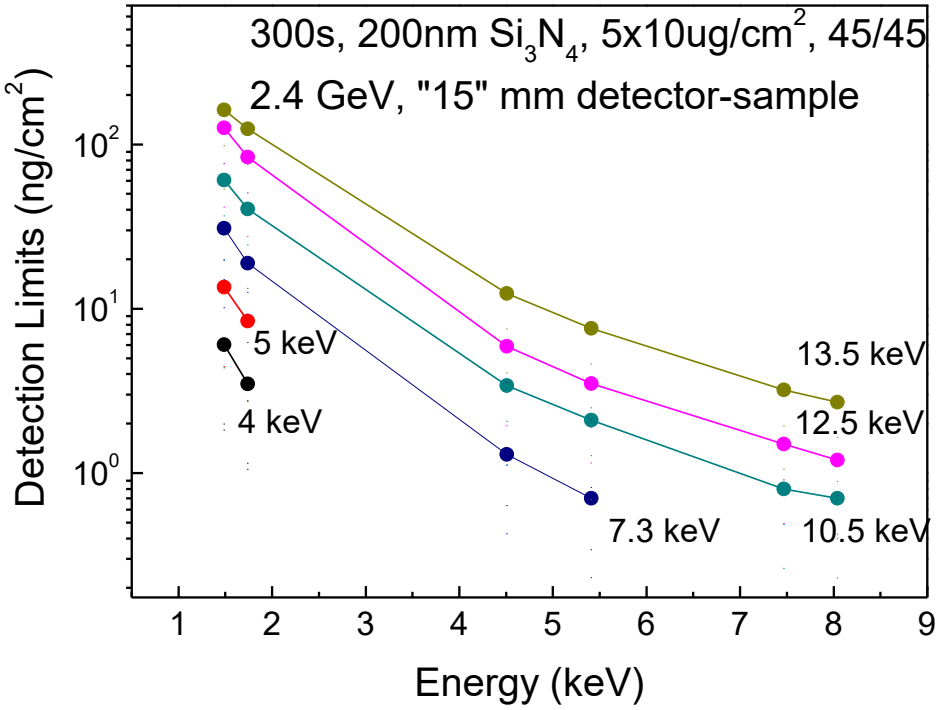

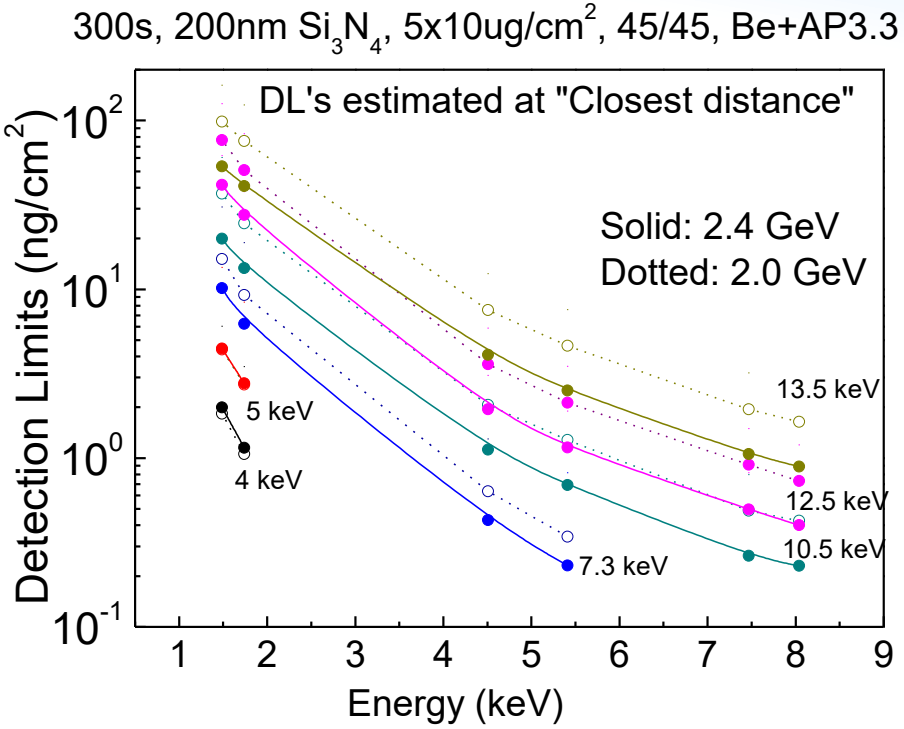

Detection limits (Al - Cu): 2 - 0.2 ng/cm²

Detector geometry for TXRF

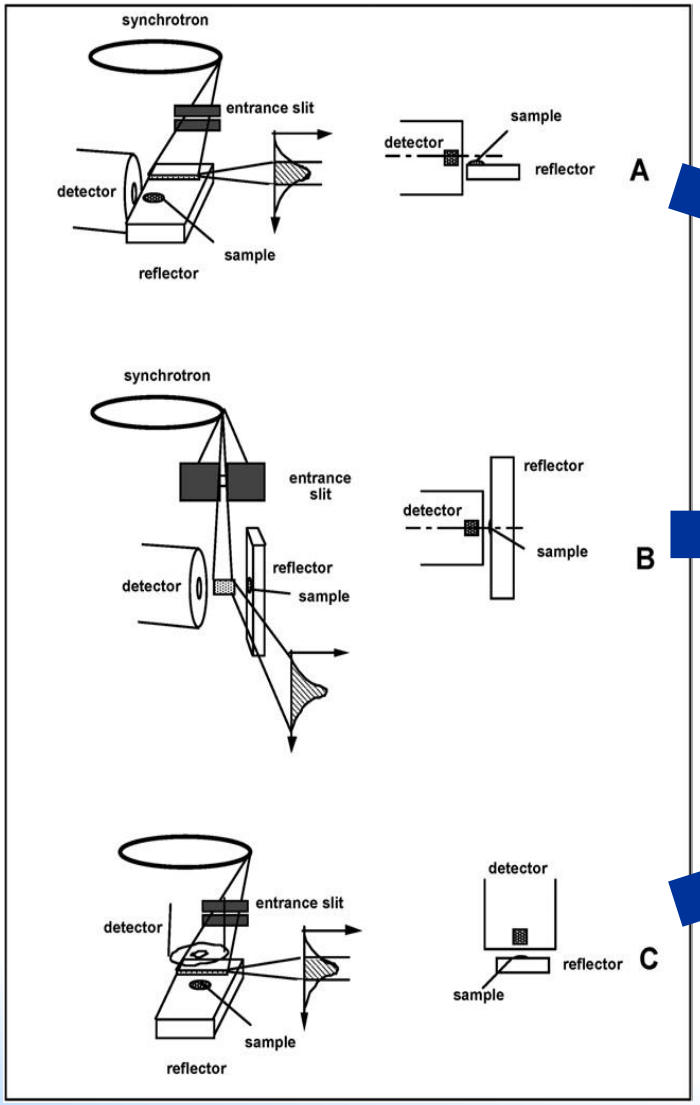

The beam is naturally vertically collimated (0.1-0.2 mrad) and has linear polarization in the orbit plane

Good excitation
No scattering
Poor detection

Poor excitation
No scattering
Good detection

Good excitation
Scattering
Good detection

C. Streli, P. Wobrauschek, F. Meirer and G. Pepponi, *Synchrotron radiation induced TXRF*, J. Anal. At. Spectrom., 2008, 23, 792–798, DOI: 10.1039/b719508g

GIXRF: C/Ti double layer

Prepared and characterized by AXO Dresden

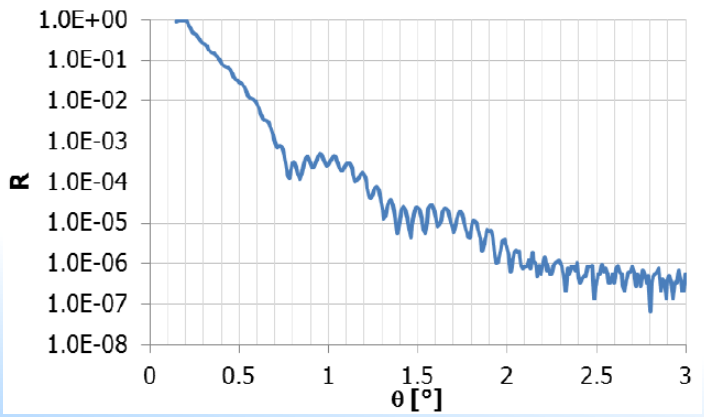

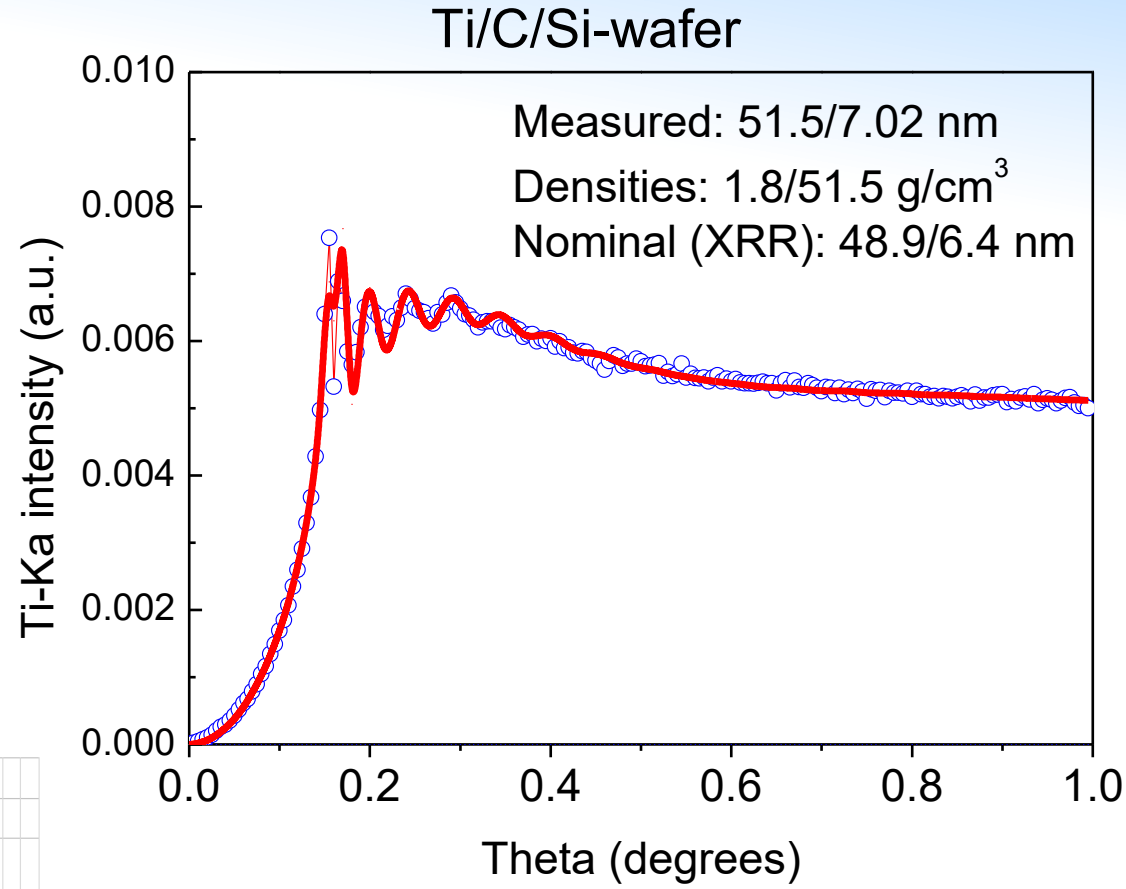

	Fit	Nominal
Ti (nm)	7.0	6.4
C (nm)	51.5	48.9

W/B_4C/ Multilayered (x15) thin film

Multilayered sample, prepared by the Ramanna Center for Advanced Technology, Indore, India

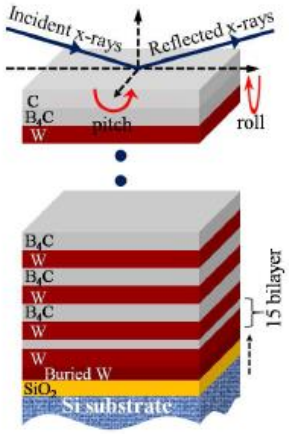

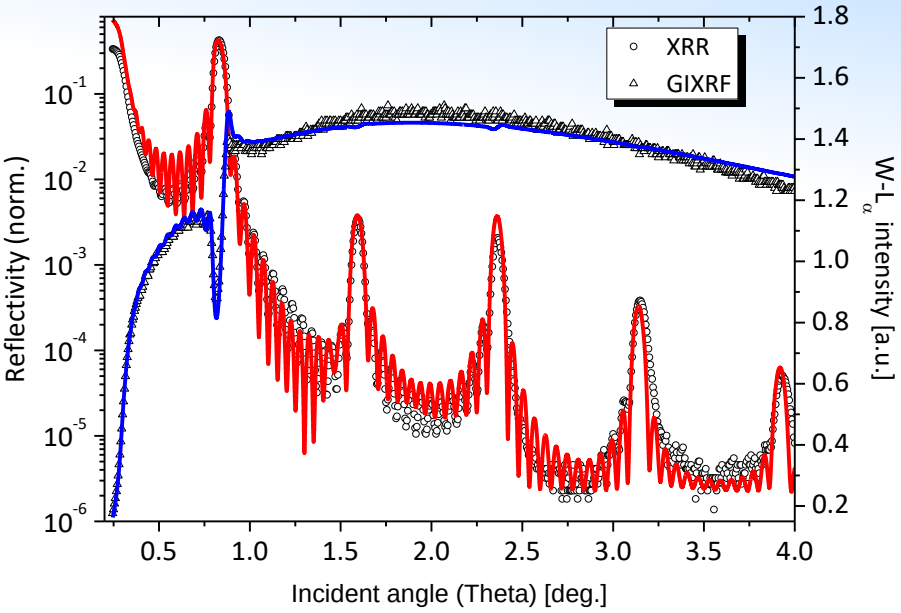

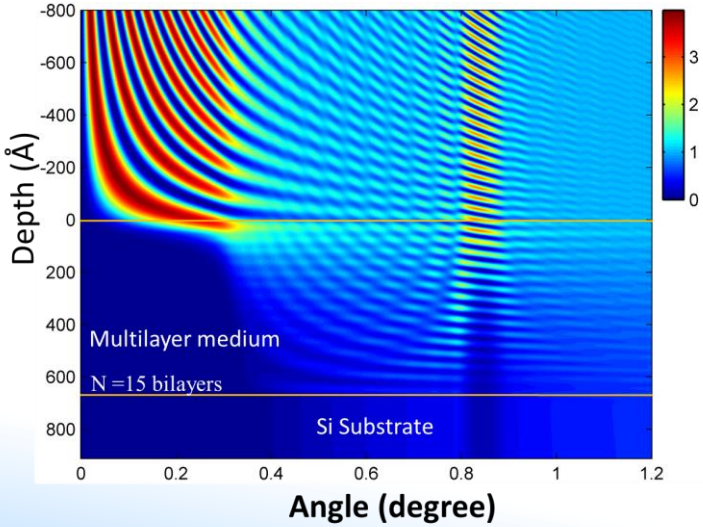

Electric Field Intensity (Normalized)

		'B4C'/'W' multilayer		
Layer Material	Periodicity	Thickness (nm)	Roughness (nm)	Density (g/cm^3)
B_4C	14	1.9 ± 0.1	0.2 ± 0.1	2.10 ± 0.2
W		2.4 ± 0.2	0.3 ± 0.1	16.0 ± 0.2
B_4C	1	2.1 ± 0.6	0.45 ± 0.2	2.3 ± 0.2
W		3.6 ± 0.3	0.55 ± 0.2	15.5 ± 1.0
SiO_2	1	2.0 ± 0.3	0.5 ± 0.2	2.0 ± 0.3

good agreement with previous analyses performed at the BL-16 beamline of Indus II

X-ray Absorption Spectroscopy

XANES: local site symmetry, oxidation state, orbital occupancy
EXAFS: local structure (bond distance, number and type of neighbors)

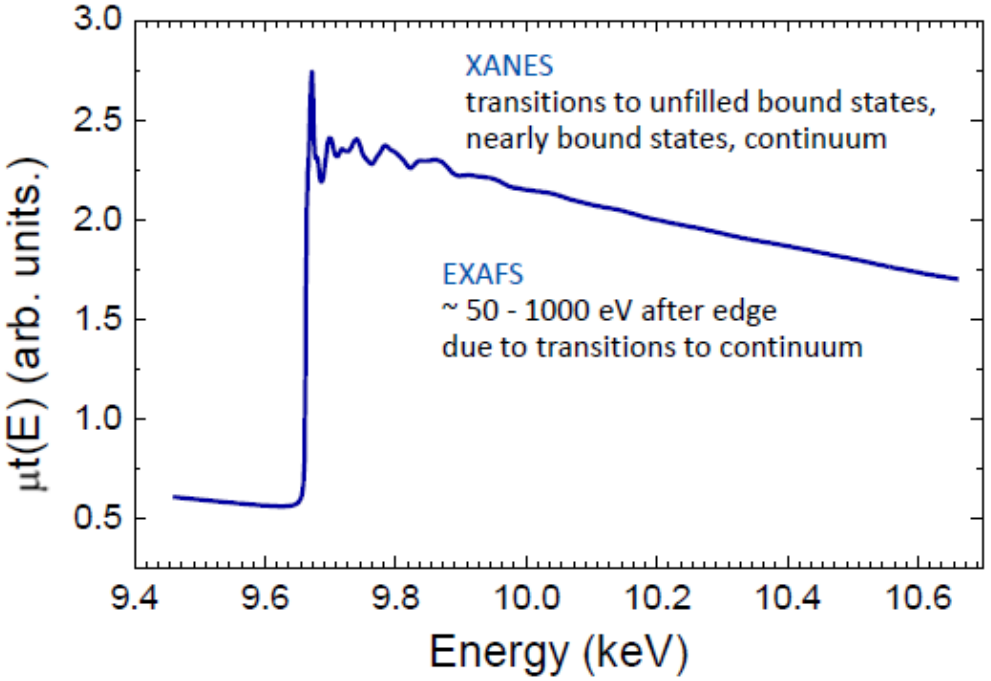

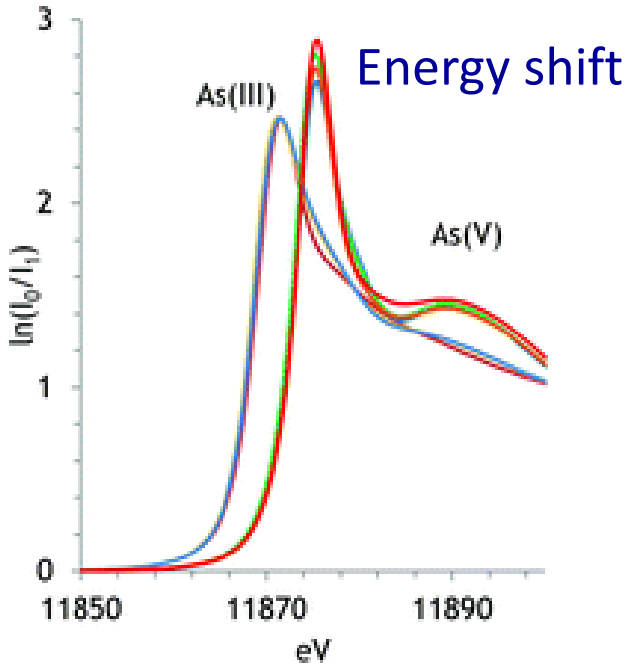

Fine structure is affected by energy and density of electronic states and transition probabilities

Extended fine structure presents oscillated pattern due to constructive and destructive interferences of the outgoing photo-e wave with neighbor atoms.

XSW assisted XANES

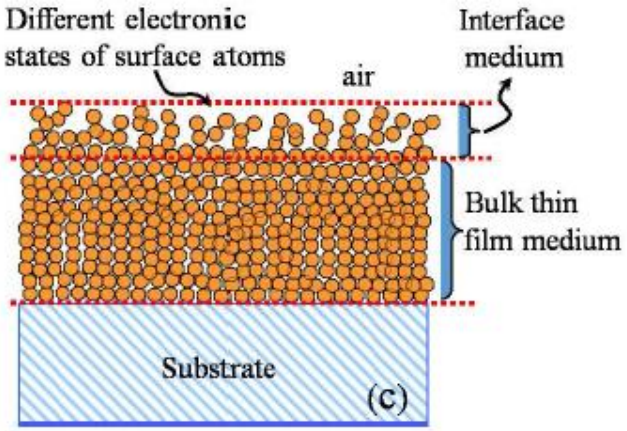

White line is the result of electron transitions from W-2p3/2 orbitals to partially filled 5d orbitals. In the case of surface or interface W-states (but also in the case of defects), transitions may occur also to unoccupied localized states near the 5d states because of lack of bulk symmetries. In this case, sharp dipolar transitions may happen between core levels and unoccupied surface states

Depth resolved speciation

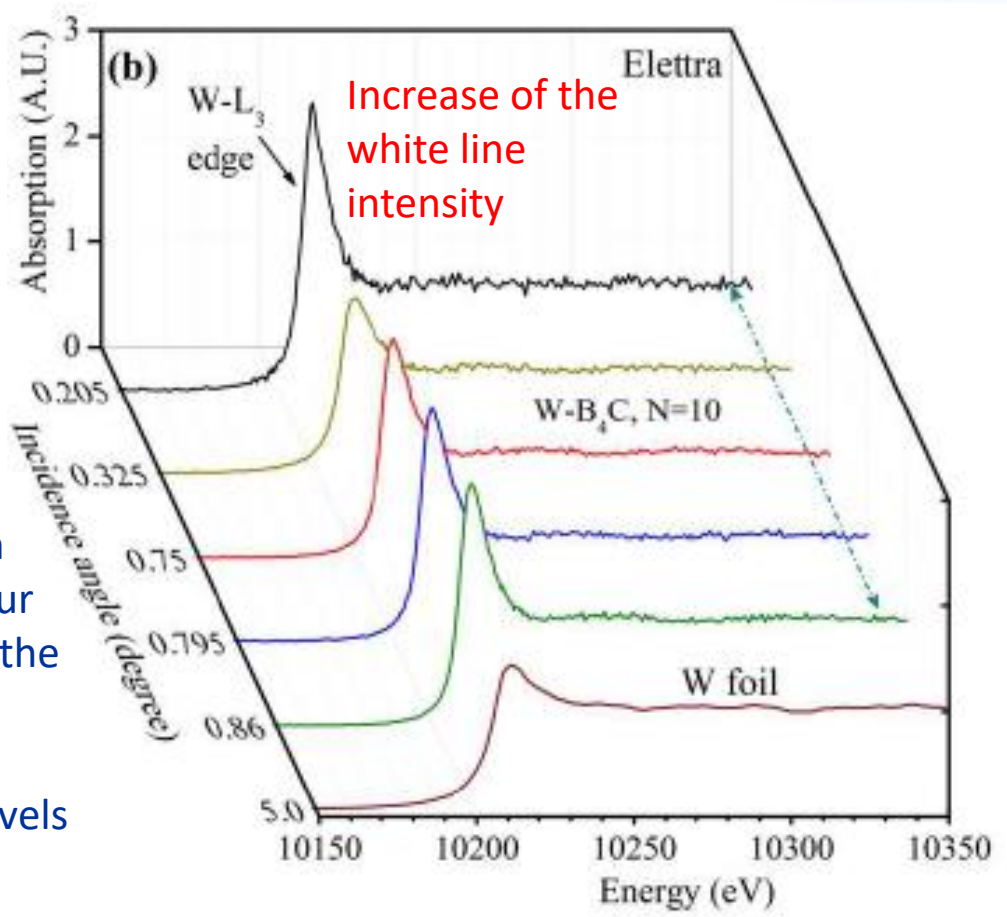

Gangadhar et al., arXiv:1705.04097v1, 11 May 2017, submitted, Phys. Rev. B'

❑ Zn speciation in fractionated APM

9-stage May-type cascade impactor

Sampling of size fractionated aerosol, down to 0.07um size 20-3200 L of air

Deposited particles form a stripe of 200-500 µm width on the 20x20 mm^2 Si wafer

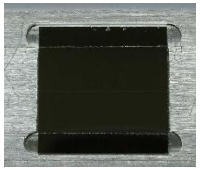

Sample geometry well suited to SR-TXRF-XANES investigations!

J. Osan, Environmental Physics Department, Centre for Energy Research, Budapest, Hungary

*Self-absorption correction as described in: Osán J et *al*., Spectrochim Acta Part B 65 (2010) 1008-1013

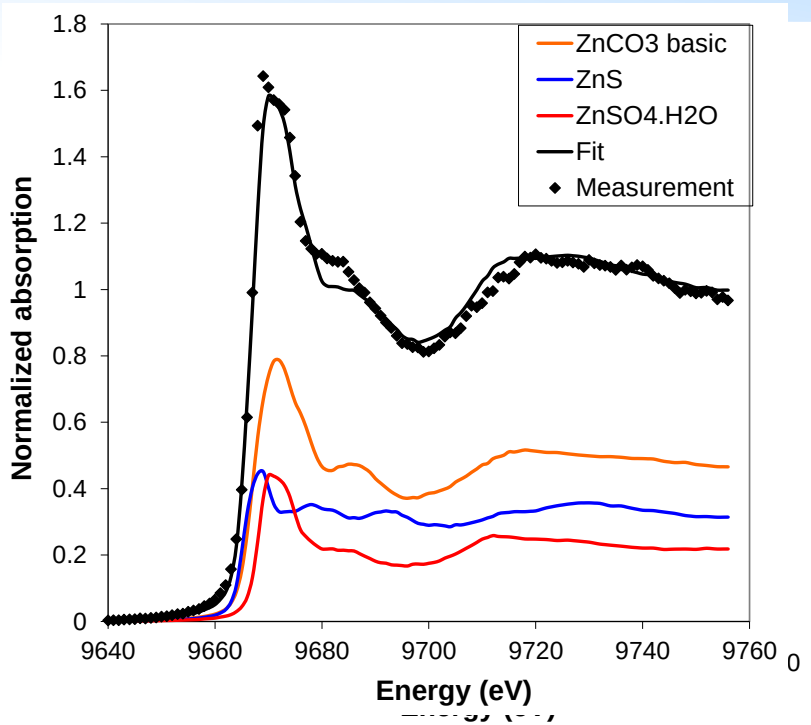

Sample: Paks (Hungary), 0.3-0.6 µm, Zn content: 74ng/m3 (284 ng on 20 mm strip)

47%-$ZnCO_3$, 32%-ZnS, 22%-Zn in glass

Main source: **Iron smelter**

Sample: Budapest (Hungary), 0.15-0.3 µm, Zn content: 239ng/m3 (884 ng on 20 mm strip)

38%-$ZnSO_4$, 40%-ZnS, 23%-Zn in glass**

Main source: **Burning of painted wood**

❑ Aerosols from 3D metal printing

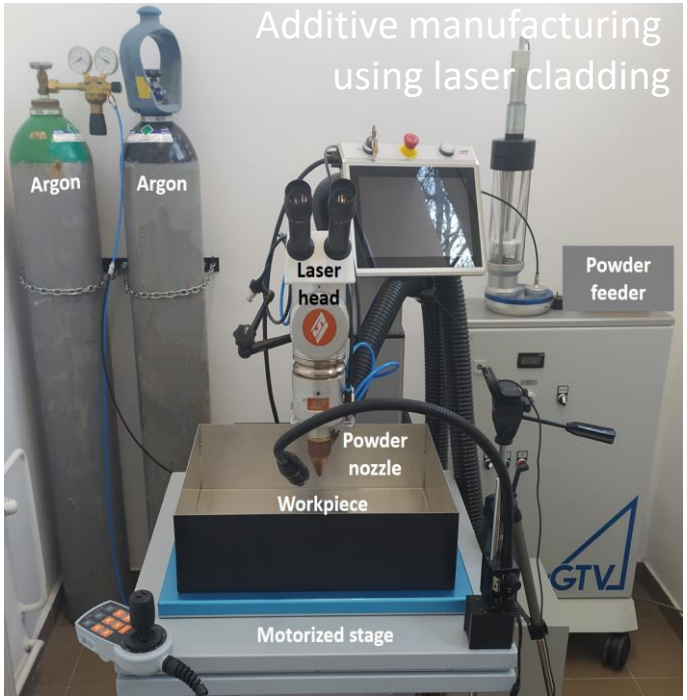

Figure courtesy: Attila Nagy, Wigner FK, Budapest, Hungary

XANES: Elettra XRF and XAFS beamlines

Cr oxidized – oxidation number ~+1.0
No significant amount of Cr^{6+} detected

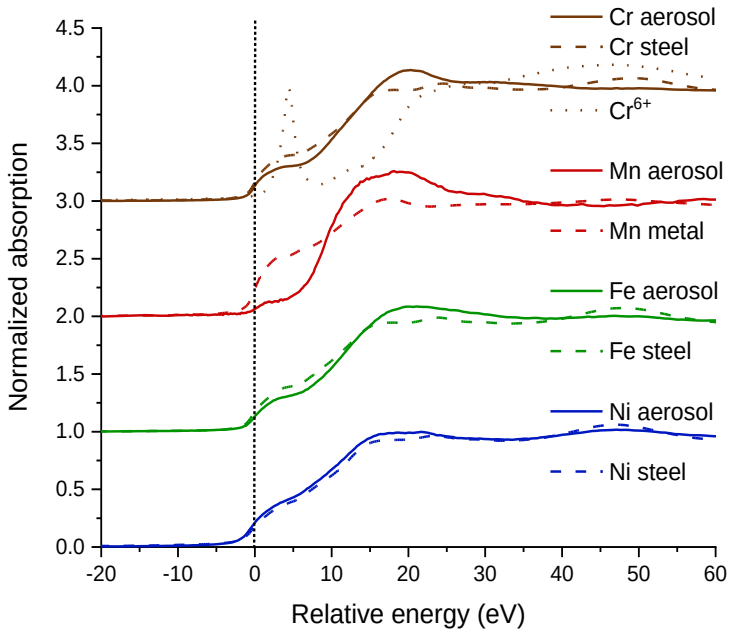

Mn mostly oxidized – oxidation number ~+2.3

Fe slightly oxidized – oxidation number ~+0.7

Ni mostly metallic – oxidation number ~+0.1

Most of emitted aerosol particles are in the ultrafine range

Oxidation number increases with decreasing particle diameter – important for estimation of health effects

S. Kugler et al., Spectrochim. Acta Part B 2021, 177, 106110

❑ Se and Hg in edible mushrooms

K. Vogel-Mikuš [1], P. Kump[2], I. Arčon[3]
[1] Biotechnical faculty, University of Ljubljana, [2]Jozef Stefan Institute,
[3] University of Nova Gorica

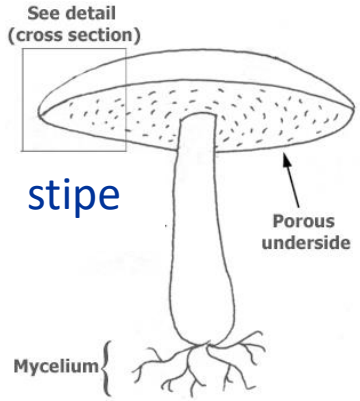

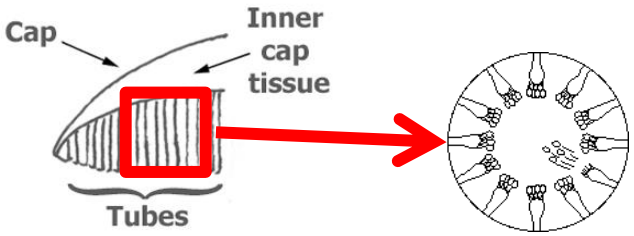

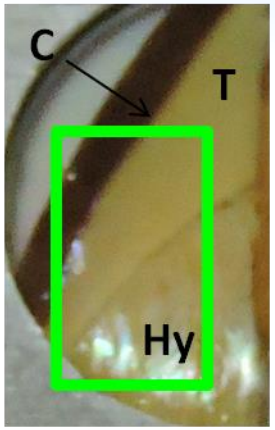

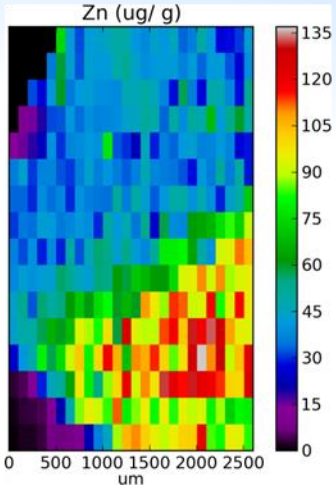

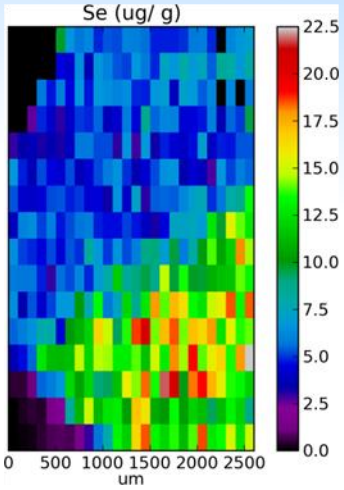

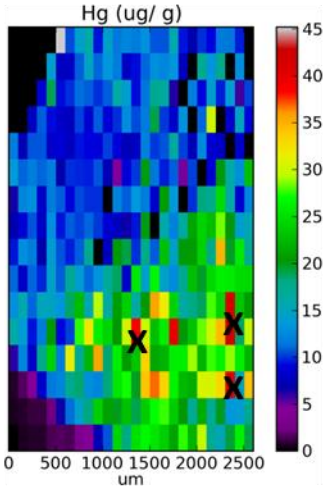

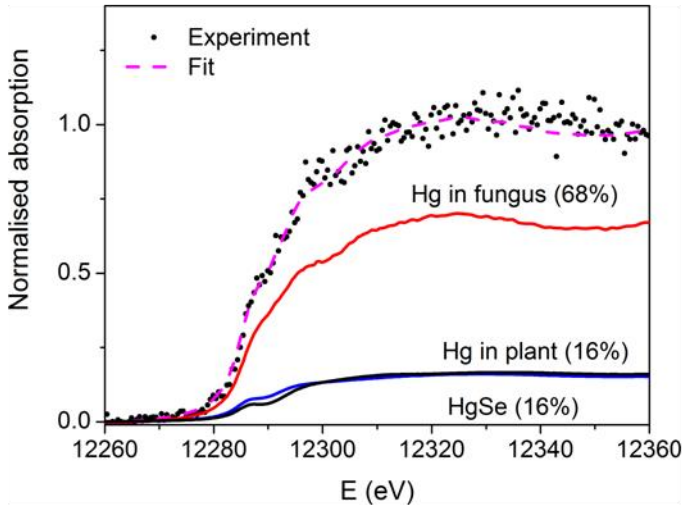

Hg is bound to tetra-cysteine proteins (metallothioneins). These proteins are digested by enzyms in the stomach and Hg is released and absorbed in our body.

GI-XANES on Black Glaze

Fe-based decorations of Ancient ceramics manufactured in South Italy

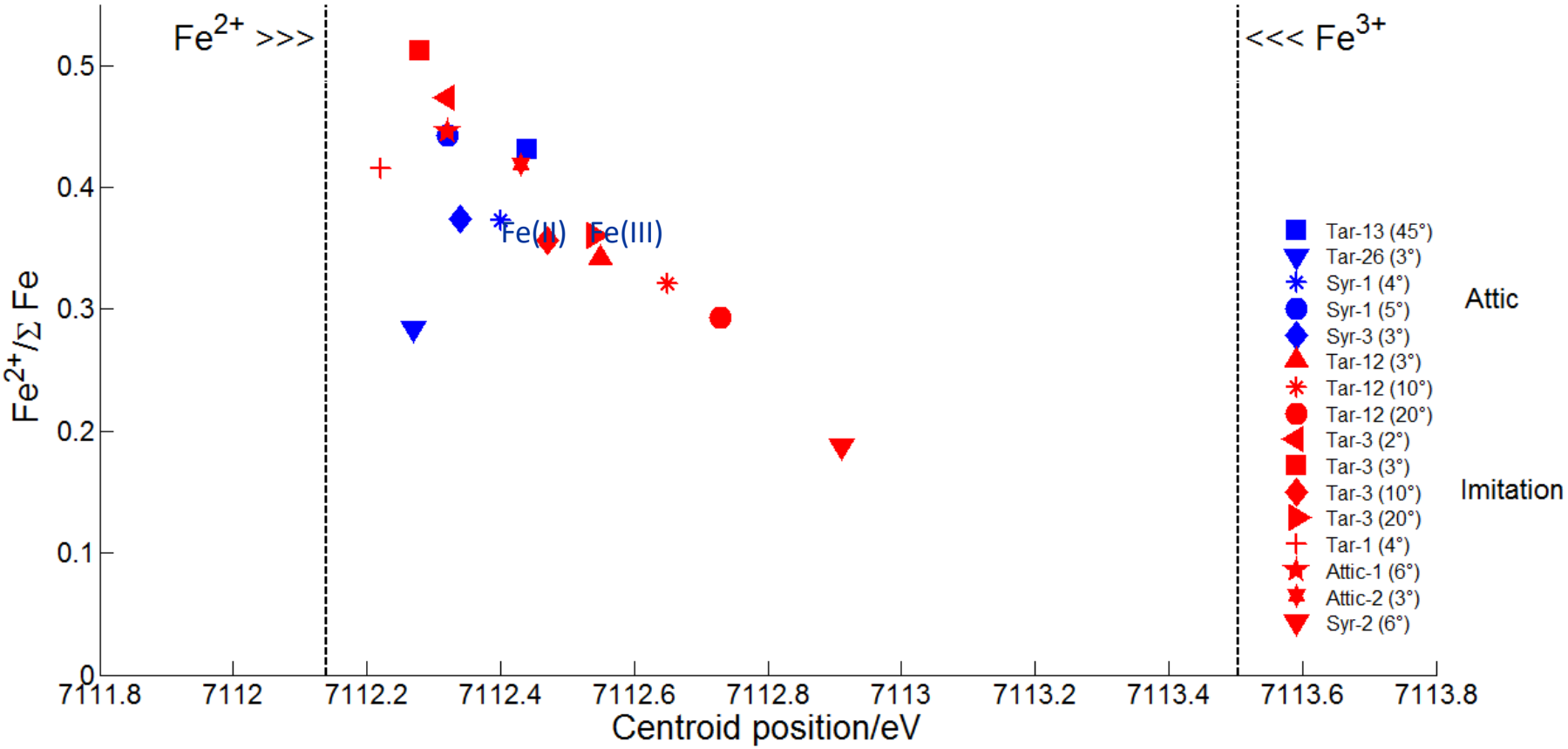

Taranto Archeological Museum Apulo f.r. Anonymous (Half IV cent. b.C.)

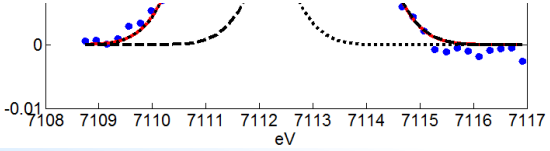

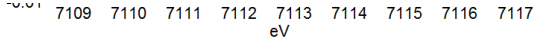

P. Romano, C. Caliri
INFN-LNS, Catania, Italy

XANES on ancient glass beads

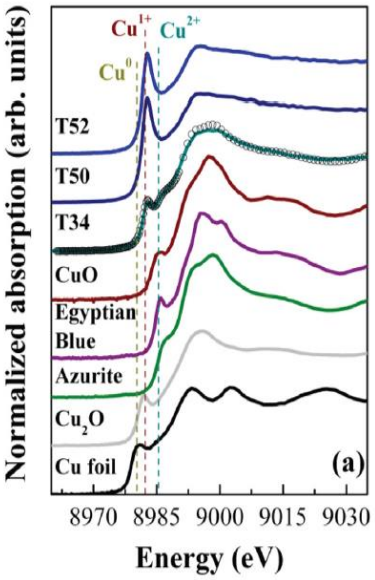

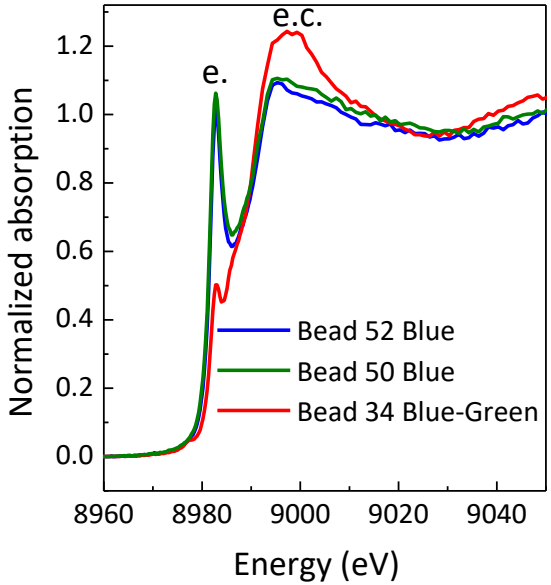

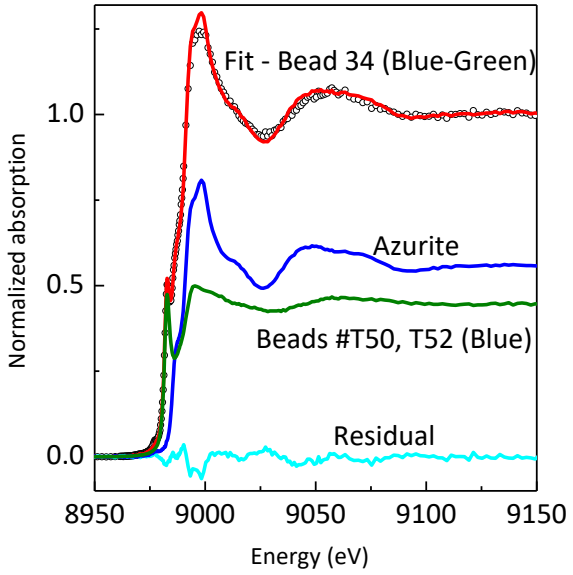

The position of the edge crest of all the samples fits with that exhibited by Cu_2O, but in the beads this feature is much broader. The dominant species in the deep blue glass samples is Cu+ dispersed in the glass alumino-silicate matrix, possibly accompanied by a minor presence of divalent copper.

Pinakidou F., *Transition metal chromophores in glass beads of the classical and Hellenistic period: Bonding environment and colouring role*, Spectrochimica Acta Part B 171 (2020) 105928

❑ Resonant inelastic X-ray scattering

Absorption edges of Pt and Au

	Pt	Au
Z	78	79
L1 (keV)	13.88	14.353
L2 (keV)	13.273	13.734
L3 (keV)	11.564	11.919

Synchrotron XRF spectra of pure (99.99%) thick (thickness 25 μm) gold samples

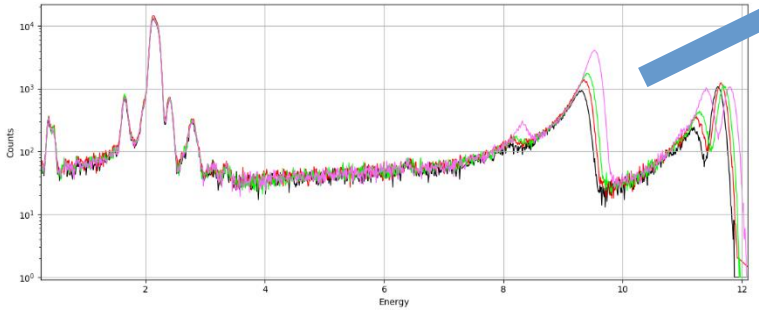

Incident energies employed: 11600, 11650, 11700, 11800 eV

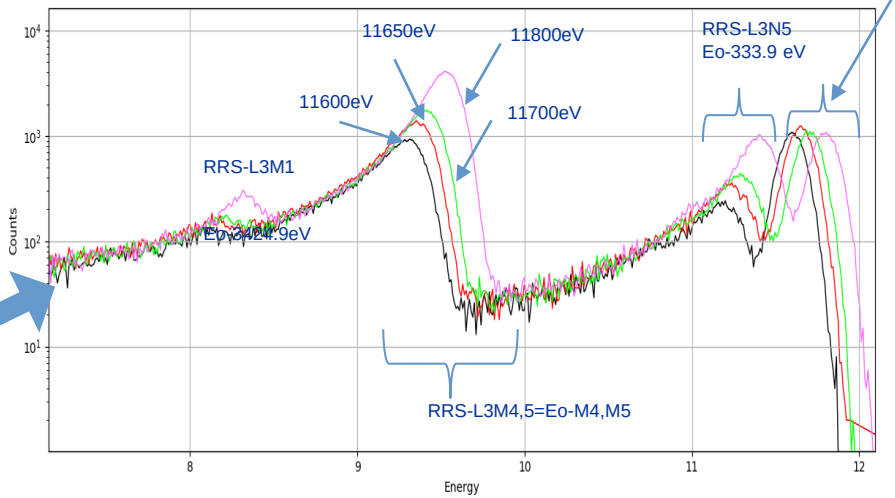

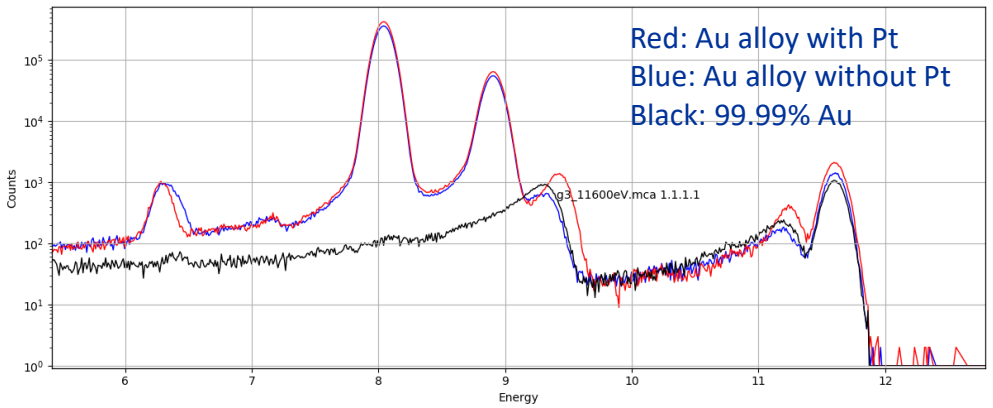

Eo=11600 eV @Elettra

Pure gold spectrum vs. Gold alloy with 0.15% Pt (Au:65.56%, Cu:25.21%, Ag:9.08%) and vs. a different certified alloy of similar composition without Pt

11600 eV > Pt(U_L3)=11564 eV

Courtesy of A.G.Karydas, (National Center for Scientific Research "Demokritos", Greece)

IAEA
International Atomic Energy Agency

Thanks for your attention!

Alessandro Migliori

a.migliori@iaea.org

https://nucleus-new.iaea.org/sites/nuclear-instrumentation/Pages/Home.aspx

https://www.elettra.trieste.it/lightsources/elettra/elettra-beamlines/microfluorescence/x-ray-fluorescence.html